Bulletin of the Seismological Society of America, Vol. 106, No. 3, pp. 904–911, June 2016, doi: 10.1785/0120150272

Source Parameter Scaling and the Cascadia Paleoseismic Record

by Anne M. Tréhu

Abstract Several approaches to interpreting the Cascadia paleoseismic record are used to derive relationships between fault area, slip, and moment and to compare the results with the scaling relationships determined by Somerville *et al.* (2015) for recent subduction-zone events. In two models (CA12a and CA12b), taken from Goldfinger *et al.* (2012), paleoevents are classified into five characteristic areas (CA), with the slip during each event estimated based on the time between the event and either the following or the previous event. In model CA14, taken from Scholz (2014), slip on four characteristic segments is determined from the plate tectonic convergence rate, assuming a constant stress drop. In model CL, introduced in this article, the fault length for paleoevents is defined by the along-strike length over which the observations have been correlated; width and slip are interpolated from model CA14. CA12a and CA12b show large scatter compared with the global compilation because of large variations in slip for a given area. Models CA14 and CL reproduce the relationship derived for asperities (defined as patches in finite-fault models with slip > 1.5 times the average slip). These models can be reconciled with the total area and average slip from Somerville *et al.* (2015) by increasing the fault area and decreasing the slip using scaling factors derived from the analysis of recent earthquakes (CLmod1) or by reducing the slip by a factor of ∼8 (CLmod2). CLmod1 implies that the paleoearthquake observations are controlled by high-slip patches, whereas CLmod2 implies that much of the plate tectonic convergence is accommodated aseismically. A scenario intermediate between CLmod1 and CLmod2 is considered most likely. This study demonstrates the value of using scaling relationships based on modern earthquakes as a tool for evaluating earthquake histories derived from paleoseismic data.

Online Material: A table summarizing the source parameters for the different models presented in this article to enable figure reproduction. Figures that summarize the data points used by Somerville *et al.* (2015), data points from a new analysis that became available after preparation of the main article (Ye *et al.*, 2016), and results for the turbidite mass model (Goldfinger *et al.*, 2012) for estimating seismic moment.

Introduction

It is generally accepted that great ($M_w \sim 9$) low-angle thrust earthquakes have occurred on the Cascadia subduction in the past, most recently in 1700, and that they will occur again in the future. Here we examine three different, related approaches to quantifying the earthquake history based on paleoseismic data and compare the implied source characteristics with scaling parameters derived by Somerville *et al.* (2015) for 44 recent megathrust earthquakes for which detailed slip models are available. Quantification of the earthquake history and source characteristics is needed to evaluate earthquake hazard, to determine probabilities for future events, and to design strategies for earthquake early warning. The three models represent different approaches to interpreting the 10,000 year Cascadia megathrust history proposed by Goldfinger *et al.* (2012), based on a synthesis of onshore and offshore paleoseismic data. This history has been used as the basis for a number of statistical analyses to forecast future earthquake activity (e.g., Kulkarni *et al.*, 2013; Petersen *et al.*, 2014; Rong *et al.*, 2014).

Scaling Relationships for Large Subduction-Zone Earthquakes

Because they contain clues to earthquake physics, there is a long history of studies documenting empirical scaling relationships between fault length, width, slip, and seismic moment in

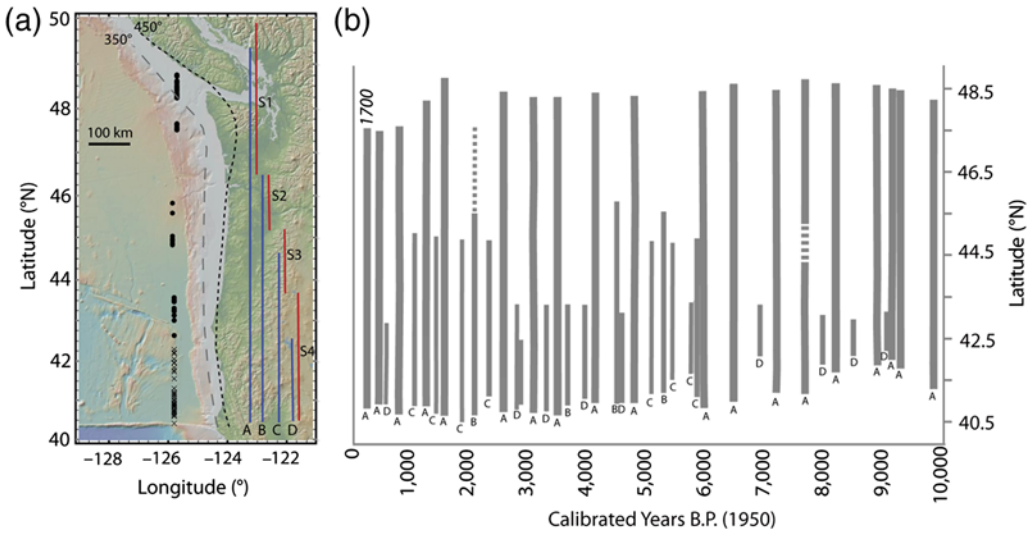

Figure 1. Paleoseismic history of the Cascadia subduction zone based on figure 52 of Goldfinger *et al.* (2012). (a) Topographic map of Cascadia. Thick vertical lines labeled A–D show the bins defined by Goldfinger *et al.* (2012); lines labeled S1–S4 are segments from Scholz (2014). Dots aligned along −126° longitude show the northern end and × symbols show the southern end of the individual correlated paleoearthquakes in (b). Dashed lines are the 350°C and 450°C isotherms on the plate boundary from the model of Hyndman and Wang (1993). (b) Vertical bars indicate the length along the margin over which geologic indicators of paleoearthquakes are observed as interpreted by Goldfinger *et al.* (2012). The length and width of the bars (including dashed segments reflecting uncertain correlations) were reproduced directly from figure 52 (pp. 99–101) in Goldfinger *et al.* (2012); letters beneath the bars indicate the bins to which each event was assigned. The color version of this figure is available only in the electronic edition.

different tectonic settings (e.g., Kanamori and Anderson, 1975; Scholz, 1994, 2002). Seismic moment is defined to be μLWS, in which μ is the shear modulus of the rocks adjacent to the fault, L and W are fault length and width, and S is the average slip and is generally estimated from the long-period seismic-wave radiation. In spite of the complexity of the factors that control slip nucleation and propagation in earthquakes, scaling properties relating radiated seismic energy to earthquake source dimensions, slip, and stress drop are remarkably robust.

Somerville *et al.* (2015) recently compiled finite-slip models for 44 subduction-zone earthquakes with $6.75 < M_0 < 9.1$ to provide constraints on hypothetical source models used to simulate ground motions expected for a future Cascadia great earthquake (Skarlatoudis *et al.*, 2015). In addition to compiling models of fault length, width, and average slip, they determined asperity area, as defined by "fault elements whose slip is 1.5 times or more larger than the average slip over the fault" (Somerville *et al.*, 2015, p. 7). When several models were available for a particular event, one solution was selected. See Somerville *et al.* (2015) for more details on the criteria used to select models and on scaling statistics derived from these data. Ⓔ Figure S1 (available in the electronic supplement to this article) illustrates the variability in the global data set and the difference between total slip area and asperity area for one particular model. Because the global data set includes earthquakes from a wide range of geological settings, including a wide range of plate convergence rates, subducting plate ages, and sediment thickness on the subducting plate, we might expect more heterogeneity than for the 10,000 year Cascadia history, which represents subduction of a very young, sediment-covered plate at a moderate rate.

Although there is considerable diversity among the earthquakes in the Somerville *et al.* (2015) database, the relationships between seismic moment and total rupture or between asperity area and average or asperity slip are generally consistent with a self-similar scaling model; removing the constraint of self-similarity did not significantly improve the fit to the data (Somerville *et al.*, 2015). Moreover, the relationships derived for models trimmed to include only the area defined as asperities are distinctly different from those derived for the total rupture area and slip. On average, the asperity area is 0.24 times the total area and the average slip on the asperities is 2.3 times the average slip, implying that ~55% of the moment release during plate-boundary thrust earthquakes is from slip on asperities as defined above.

Three Related Models for Interpreting the Paleoseismic Record

The 10,000-year-long earthquake history of Cascadia reconstructed by Goldfinger *et al.* (2012; hereafter referred to as G2012) is the foundation for all of the models considered here. This history is summarized in Figure 1. Figure 1a shows the rupture segmentation assumed by models CA12a, CA12b, and CA14 (characteristic areas [CA]) in map view, as well as the calculated position of the 350°C and 450°C isotherms (Hyndman and Wang, 1993), which have guided initial estimates of fault width for all of the models. Figure 1b shows the distance along strike for which observations have been correlated by G2012 to define individual paleoearthquakes as a function of time and was constructed by removing the individual data points from figure 52 of G2012 (pp. 99–101), leaving only the

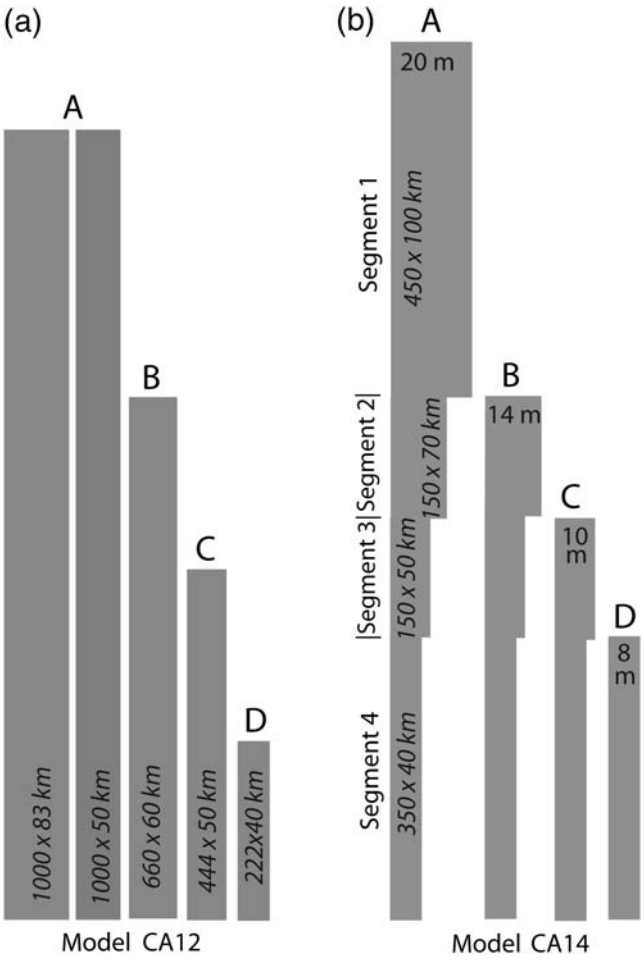

Figure 2. Fault areas assumed by Goldfinger *et al.* (2012) and Scholz (2014). The slip for each segment in the Scholz (2014) model is also shown.

interpretation of the complied onshore and offshore data. The length of these bars was used to define rupture lengths for model CL, introduced in this article. The northern (black circles) and southern (crosses) end points for each interpreted event are shown on Figure 1a. G2012 estimate that the along-strike length over which an event is observed may overestimate the length of the rupture by as much as 90 km at each end. On the other hand, observations are not continuous along strike, and an event could have extended farther along strike than indicated by the observations. Because these two poorly quantified sources of uncertainty have a competing effect, we did not attempt to incorporate them into this analysis. We also do not consider the possibility that some of the interpreted long ruptures may actually represent a series of shorter, contiguous ruptures closely spaced in time or that some events may be missing from this record, as discussed by Atwater and Griggs (2012), although such scenarios can be explored within the framework presented below, as can updated versions of the along-strike extent of event correlations.

G2012 interpreted the earthquake history shown in Figure 1 to reflect a scenario in which all paleoearthquakes can be assigned to one of four characteristic lengths (A–D in Fig. 1). All of the characteristic lengths have their southern boundary at the Mendocino Triple Junction, although the observed southern limit for individual events spans a distance of ~200 km. This interpretation results in considerable variability in the correlated length within each characteristic length bin and in overlap between bins (Fig. 1a). G2012 assumed a constant fault width for each bin (with two different fault widths being assumed for type A events, depending on the time since the previous type A event). Figure 2a is a scaled illustration of this characteristic area model, which will be referred to as model CA12. G2012 calculated the slip for each type A event based on the time to the next event and calculated the moment and moment magnitude for each type A event in the record based on this slip, the characteristic area, and an assumed shear modulus of 30 GPa (C. Goldfinger, personal comm., 2015). For type B–D events, the slip was calculated by averaging the slip derived for the type A events and that derived from the time difference between type B–D events using a formula that combined times of previous and following events (see table 8 of G2012, p. 90). Because the moment value for a particular type B–D event in table 8 is not always consistent with the values of length, width, and slip given for that event, we refer to relationships derived using the moment values in table 8 as model CA12a. Model CA12b uses moments recalculated using the length, width, and slip given in the table; for consistency with the two approaches presented below, a shear modulus of 40 GPa was assumed for CA12b.

Scholz (2014) presented an alternative model, referred to here as CA14, which includes four characteristic lengths with segment boundaries that are somewhat different from those of G2012. In contrast to model CA12, fault width for CA14 varies in segments 1–4 toward the south (Figs. 1a and 2b). Slip values were calculated to be consistent with the plate tectonic convergence rate and the constraint of constant stress drop. Like CA12, this model includes 19 type A events, which include fault patches defined by simultaneous rupture of segments 1–4, interspersed with shorter ruptures aligned on their southern end with the Mendocino Triple Junction and composed of segment 4 for type D ruptures, segments 3 and 4 for type C ruptures, and segments 2–4 for type B ruptures. For model CA14, an effective fault width and slip for each event was calculated as a length-weighted average of the width and slip for each segment. The total moment (TM) release for model CA14 (assuming a shear modulus of 40 GPa) is consistent with a fully coupled plate boundary (Scholz, 2014).

Because earthquake histories long enough to include several earthquake cycles are often visualized by showing the along-strike position of the rupture zone based on historical accounts of strong shaking as a function of time (e.g., Comte and Pardo, 1991; Scholz and Campos, 2012), it seemed useful to examine the implications of taking a step backward from characteristic area interpretations to explore a model in which event length is based on the length over which observations can be correlated, referred to here as the correlated length, or CL, model. Correlated lengths are analogous to the

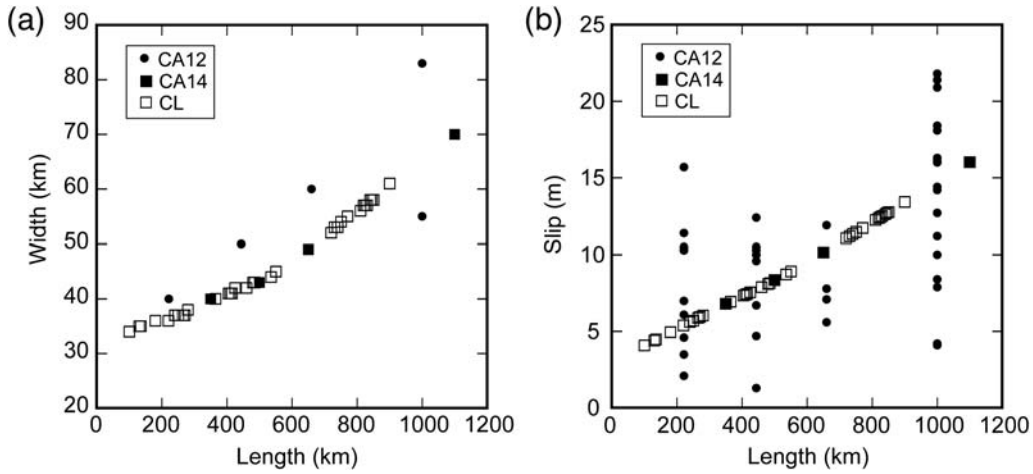

Figure 3. Relationship (a) between fault length and width and (b) between fault length and slip for models CA12, CA14, and CL (characteristic areas [CA]). Fault width and slip for model CA12 were taken from table 8 of Goldfinger *et al.* (2012, p. 90) and are the same for models CA12a and CA12b. Fault width and slip for model CA14 was calculated from the length-weighted average of the width and slip of individual segments shown in Figure 2. Fault width and slip for model CL were interpolated from the values for model CA14 based on the correlated length for each event. Fault width and slip for models CLmod1 and CLmod2 are not shown but are derived from those for model CL as discussed in the text.

fault length defined by historical observations. The approach of Scholz (2014) was used to estimate fault area and slip as a function of correlated length by interpolating the length versus width or slip functions determined for model CA14. A shear modulus of 40 GPa was assumed for moment calculations.

Figure 3 shows the relationship between the fault length and the effective width and slip for models CA12, CA14, and CL. Average rupture widths are narrower in the CA14 and CL models compared with CA12, with the exception of the three type A events with a width of 50 km in CA12. The most striking difference between CA12 and CA14 or CL, however, is the relationship between average fault slip and length (Fig. 3b). For CA12, the slips vary widely for events of a given length, implying large variations in stress drop between events. For the CA14 and CL models, the slip varies smoothly with length based on the plate tectonic rate and constraint of constant stress drop. The generally shorter fault lengths for the CL model compared with CA models reflect relaxation of the constraint that the Cascadia subduction zone is fully coupled for its entire length, as discussed below.

Scaling Relationships Implied by the CA12, CA14, and CL Models

Figure 4 shows the calculated moment versus area and moment versus slip for the CA12, CA14, and CL models compared with the self-similar scaling relationships derived by Somerville *et al.* (2015) for modern subduction earthquakes. Because the physical processes underlying paleoearthquakes should be similar to those of modern earthquakes (Wang *et al.*, 2013), we expect the scaling relationships implied by models for the paleoearthquake history to follow scaling rules determined from modern earthquakes.

For the CA12a and CA12b models, data points for individual paleoearthquakes define horizontal lines corresponding to each of the five different characteristic areas in the model (Fig. 4a) and span nearly an order of magnitude variation in moment for each characteristic area. This is due to the variability in the derived slip for a particular rupture length in models CA12a and CA12b (Fig. 3b). For the slip-versus-moment relationship (Fig. 4b), the data points for model CA12b fall along diagonal lines corresponding to the five characteristic areas, but the data points for CA12a show the expected structure only for type A events, with unstructured scatter for type B–D events because of the complex algorithm used to derive the slip used in the moment calculation for this model (C. Goldfinger, personal comm., 2015). The scatter in the moment-versus-slip relationship for models CA12a and CA12b is greater than the scatter in the modern data. Although some scatter in this relationship is expected, it is likely that errors in the radiocarbon dates and in the algorithms used to derive slip from the time to past and future earthquakes contribute to this scatter.

The CA14 and CL models both lead to scaling relationships for both area and slip versus inferred moment that are similar to the modern relationships for asperity area (Fig. 4c) and average slip on asperities (Fig. 4d) rather than total area and average slip. The lack of scatter for these models is due to the assumptions made to derive width and slip from assumed (CA14) or correlated (CL) length. Systematically perturbing the source parameters can provide insights into why these models lead to fault areas that are more compact and slips that are larger than those for modern earthquakes.

Figure 4c,d shows the impact of two possible perturbations to the CL model. The effect of these perturbations on CA14 is not shown but is similar. For CLmod1, the area for each event was multiplied by the ratio of total area to asperity area derived by Somerville *et al.* (2015), and the slip was multiplied by the ratio of total slip to asperity slip (4.17 and 0.43, respectively). CLmod1 results in an increase in the

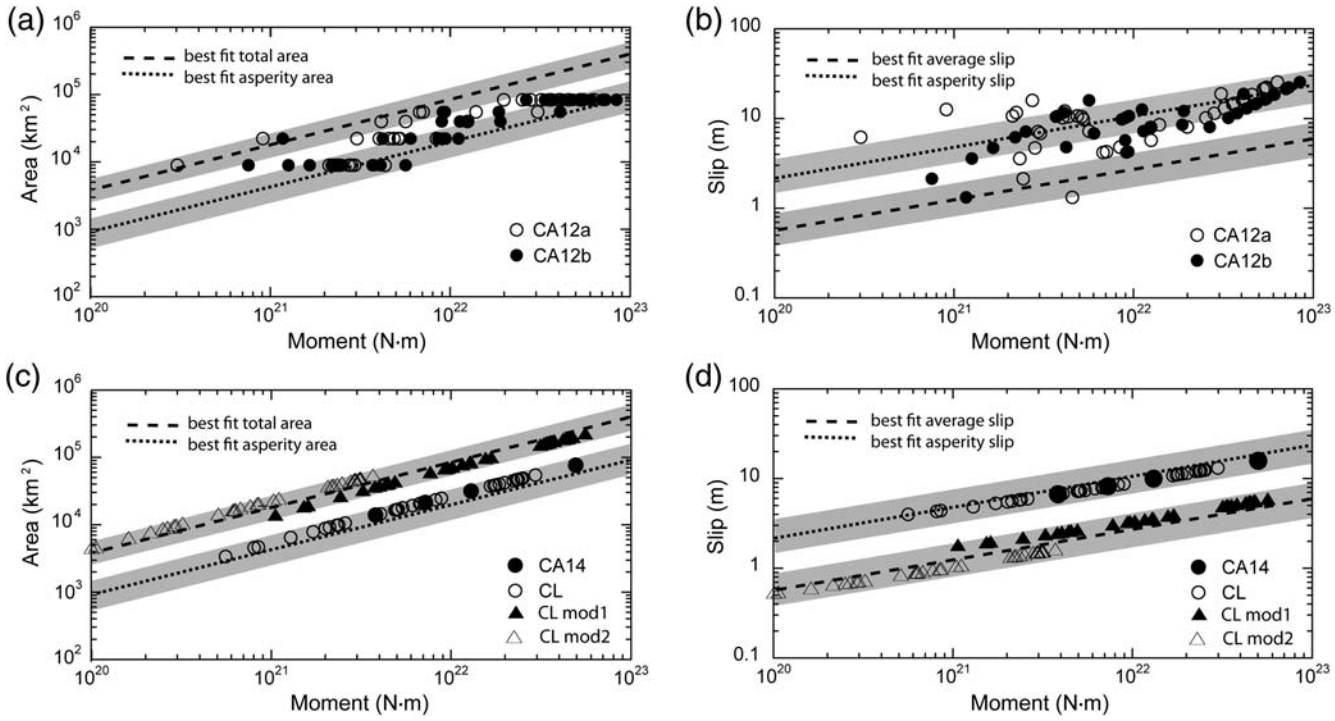

Figure 4. Scaling relationships implied by the models presented here to interpret the paleoseismic record, compared to the scaling relationships derived for large modern subduction-zone earthquakes by Somerville *et al.* (2015). Lines show the best fit to the data under the constraint of self-similarity for total area, asperity area, average slip, and average slip within asperities; gray bands show the 95% confidence limits. For the modern earthquakes, the *x* axis is the seismic moment derived from long-period seismic waves. For the six models derived from the Cascadia paleoseismic interpretation of Goldfinger *et al.*(2012; G2012), moment was calculated from estimates of fault area and slip, as described in the text. Model CA12a assumed a shear modulus of 30 GPa; 40 GPa was assumed for the other models.

calculated moment of paleoearthquakes and in scaling relationships that are similar to those determined from modern subduction earthquakes. The small difference in the slope of the observations compared with the slope of the best-fit line for modern earthquakes suggests a moment dependence of the ratios, but the effect is minor. For CLmod2, the fault dimensions for the CL model were not changed, and the slip was decreased by a factor of 8. This results in a large decrease in the calculated moment but also is consistent with scaling relationships between moment and total area or average slip. Of course, many other combinations of systematic perturbations to the area and slip are possible between these two end members. CLmod1 implies that the geological indicators of paleoearthquakes are sensitive primarily to slip on the asperities and that they underestimate total fault area and moment. In contrast, CLmod2 implies a significant amount of aseismic slip. These inferences are discussed in the context of other observations in the Discussion section.

Figure 5 shows the distribution of moment magnitudes for the six models shown in Figure 4. The TM released in 10,000 years in units of 10^{22} N·m is given in the upper right corner of each histogram. Models CA12b, CA14, and CLmod1 all indicated a TM of $\sim 10^{24}$ N·m, which corresponds to the moment release predicted by the plate tectonic convergence rate, assuming that all of the plate motion occurs in earthquakes (Scholz, 2014). The 76% lower TM release for CA12a can be attributed to the 75% lower assumed shear modulus for that model. The 50% lower TM release for CL can be attributed to underestimation of total area or to aseismic slip. CLmod2 implies that ~94% of the slip is accommodated aseismically.

The *b*-values calculated from these models following the maximum-likelihood method of Aki (1965), as presented by Naylor *et al.* (2010) and assuming a magnitude of completion of 8.2 (7.2 for CLmod2), are also shown in Figure 6. These *b*-values are consistent with the young, buoyant-plate end member in the global compilation of Nishikawa and Ide (2014). The validity of these *b*-value estimates, however, is questionable because none of these interpreted earthquake histories follows a Gutenberg–Richter distribution. If some of the type A events were actually a series of smaller events, the magnitude–frequency distribution would approach a Gutenberg–Richter distribution. This type of perturbation could be easily implemented for models CA and CL.

Discussion

The differences in the TM release calculated from the different models can be evaluated in the context of what can be inferred about the behavior of the Cascadia megathrust from other types of observations, including constraints on the down-dip limit of the seismogenic zone (e.g., Hyndman, 2013; Peterson *et al.*, 2014; Wang and Tréhu, 2016), the degree of

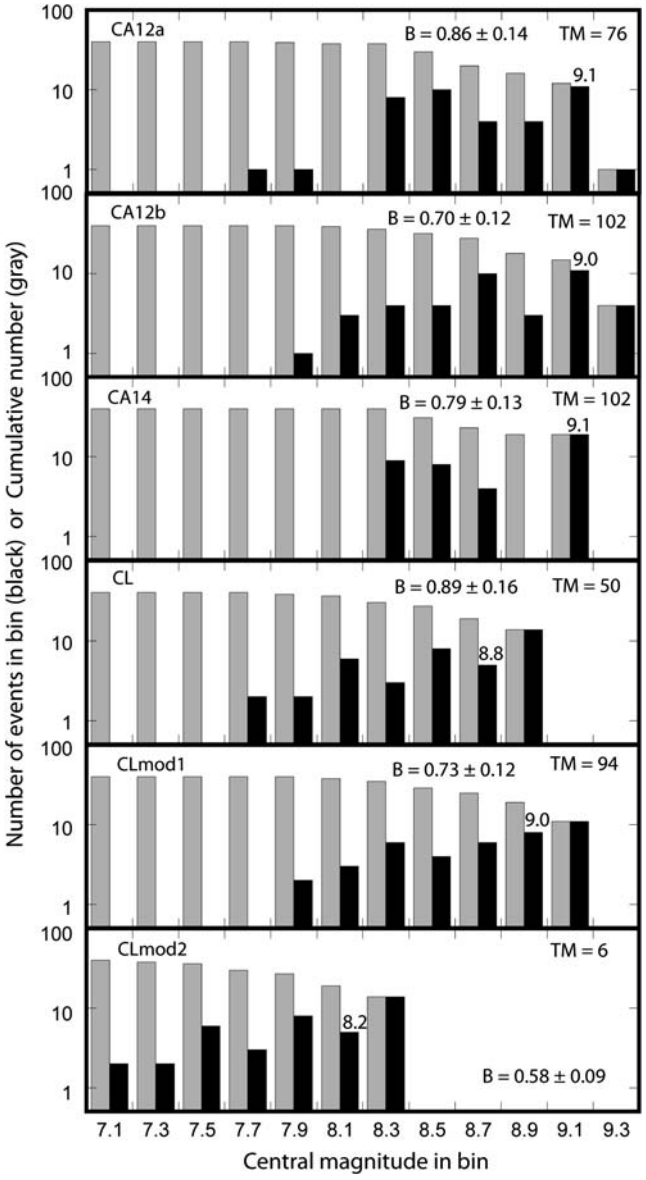

Figure 5. Number (black) and cumulative number as a function of moment magnitude for the six models shown in Figure 4. The total moment (TM) for the 10,000-year history is shown in units of 10^{22} N·m, as are *b*-values calculated by the method of Aki (1965) following Naylor *et al.* (2010) and the moment magnitude for the 1700 earthquake implied by the model.

coupling along strike as constrained by geodetic data (e.g., McCaffrey *et al.*, 2007; Burgette *et al.*, 2009; Schmalzle *et al.*, 2014), and constraints on the moment, subsidence, and slip distribution of the 1700 earthquake (e.g., Satake *et al.*, 2003; Leonard *et al.*, 2010; Wang *et al.*, 2013).

Models CA14 and CL both reproduce the scaling relationship between moment and asperity area or average asperity slip. We have shown that multiplying the area and slip in model CL by factors derived from the modern data set (CLmod1) produces a scaling relationship between moment and total area or average slip that is similar to that for modern earthquakes. Because the TM release for model CLmod1 is the same as the moment release for model CA14 and because the same approach was used to define width and slip as a function of length, CA14 can be interpreted to be a schematic simplification of data-based model CLmod1, which implies that the observed correlation lengths of model CL reflect slip on asperities and that essentially all plate tectonic convergence is manifested by seismogenic slip in a relatively wide, thermally controlled zone. This explanation leads to the question of whether increasing the area of the paleoruptures in model CL by a factor of ~4 (accompanied by a decrease in slip by a factor of 2) is compatible with other constraints on the maximum area of the plate boundary that ruptures in large earthquakes. Figure 6 shows the model rupture extent for CA14 in map view, assuming an average plate dip of 10°, with segment 1 split into two rectangles to accommodate the bend in the subduction zone. The up-dip limit of tremor accompanying episodes of slow slip (Boyarko *et al.*, 2015) and the 100 and 30 mm contours of the total slow slip for 2005.5–2011 in the model of Schmalzle *et al.* (2014) are also shown. Assuming that the maximum fault length is 1100 km, the length of the longest event in the CL model can be increased by a factor of 1.22, requiring an increase in width by a factor of 3.28 and yielding an average fault width of 200 km. For the average correlated length of the type A events (804 km), the maximum increase in length is by a factor of 1.37, and the width must increase by a factor of 2.92–163 km. This model therefore implies that seismogenic slip during large earthquakes extends well into the zone characterized by episodic tremor and slip (Fig. 6). Whether this is possible is a matter of considerable debate; see Wang and Tréhu (2016) for a discussion of various arguments for defining the down-dip limit of seismogenic slip. Considering those arguments, it is likely that model CLmod1 has a width problem, although it is difficult to say by how much. This excess width problem can be mitigated by considering that the rupture areas of modern earthquakes may be overestimated and the average slip underestimated because of smoothing imposed on the inversion solutions. Introduction of a small amount of creep within the nominally seismogenic zone would also decrease the required fault widths.

The models predict different moment magnitudes for the 1700 earthquake, which was estimated by Satake *et al.* (2003) to have been $8.7 < M_w < 9.2$, based on modeling of tsunami observations in Japan. Models CA12a, CA12b, CA14, CL, and CLmod1 all fall within this range. For model CLmod2, however, M_w for the 1700 event is 8.2. This is only compatible with data for the 1700 tsunami if the event was a "tsunami earthquake" that generated a tsunami larger than expected from the seismic energy release. Because of the rarity of tsunami earthquakes and the lack of evidence for microseismicity or other offshore slip indicators that would be expected if 94% of the plate tectonic convergence were being accommodated through creep, as indicated by the TM release calculated from CLmod2, this model is considered unlikely. Further decrease in the uncertainty of coastal subsidence observations (Wang *et al.*, 2013) and better constraints on the

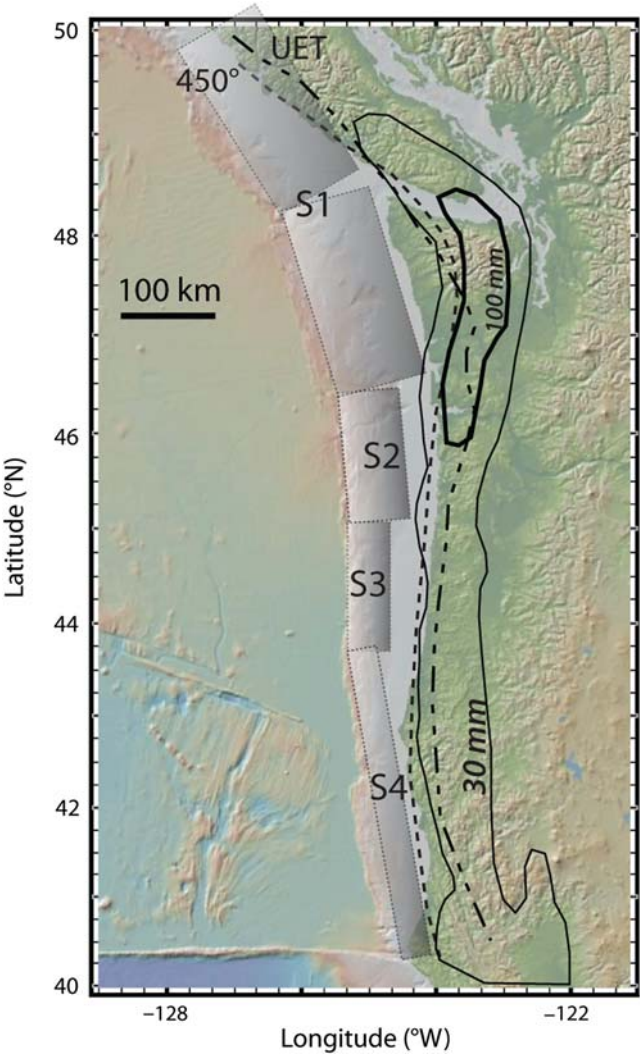

Figure 6. Cascadia subduction zone showing the rupture surface for model CA14, the up-dip extent of seismic tremor that accompanies slow slip (UET) (from Boyarko *et al.*, 2015), the 450°C isotherm (from Hyndman and Wang, 1993), and the 30 and 100 mm contours for total slip accumulated during slow slip events from 2005.5 to 2011 (from Schmalzle *et al.*, 2014). Although slip during large plate-boundary earthquakes may extend into this zone, a significant fraction of the anticipated plate convergence is currently being taken up here during episodes of tremor and slip, especially beneath northwest Washington and southern British Columbia (Chapman and Melbourne, 2009). The color version of this figure is available only in the electronic edition.

seismic energy required to generate the observed paleoseismic signals is needed to definitively rule out this possibility.

Conclusions

Although there is strong evidence that large megathrust earthquakes have occurred in the past in Cascadia and will occur in the future, there are large uncertainties associated with estimating the magnitudes and interevent timing of paleoearthquakes. The large scatter in the moment-versus-slip relationship for models CA12a or CA12b, when compared with the scaling relationship derived for recent megathrust events, suggests problems with the slip estimates for these models. Models CA14 and CL are consistent with modern scaling relationships between moment and asperity area or average asperity slip and can be perturbed to fit the scaling relationship for total area and average slip by systematically manipulating fault width and slip. Two end member models were explored, CLmod1 (scaling rupture area and slip relative to asperity area and asperity slip using factors derived from the modern data) and CLmod2 (decreasing slip, thus relaxing the assumption that plate convergence is accommodated solely through earthquakes). CLmod1 leads to fault widths that may be incompatible with physical controls on the depth extent of seismogenic rupture. Including possible biases in the modern estimates due to smoothing and allowing a few percent creep, however, could mitigate this width problem. Given uncertainties in how deep dynamic slip extends during large plate-boundary earthquakes and in how smoothing affects the total area that slipped for modern finite-fault models, a quantitative exploration of additional perturbations to CLmod1 is premature. CLmod2 requires that the 1700 earthquake to have been a tsunami earthquake and for ~94% of plate motion to have been accommodated through creep, both of which are unlikely but not ruled out.

This study demonstrates how compatibility with scaling relationships between source parameters derived for modern subduction-zone earthquakes can be used to evaluate and constrain models for paleoearthquake histories and provide insights into strengths and weaknesses of various models. It also shows that the correlated length approach to estimating paleoearthquake rupture lengths, which is analogous to earthquake history representations based on historic reports of shaking, is a useful and flexible tool that is well suited to testing interpretations. Binning the observations into a small number of characteristic areas, rather than allowing what may be natural variability in rupture length, may distort the earthquake history. Ultimately, improved characterization of the great Cascadia earthquake of 1700, better constraints on the moment and timing of paleoearthquakes (e.g., A. Lindh, unpublished manuscript, 2016), an increased and improved database of modern slip distributions, and a better understanding of the rupture process and the interplay between repeated earthquakes and geologic structure, derived from studies of subduction-zone earthquakes globally, are needed to better understand the inferred paleoearthquake history.

Data and Resources

All data were taken from Goldfinger *et al.* (2012), including their figure 52 (pp. 99–101) and table 8 (p. 90), and from Somerville *et al.* (2015, their tables 1 and 2). Although an updated characteristic area model with additional bins has recently been circulated informally (C. Goldfinger, personal comm., 2015), the underlying data to support this model have not been finalized and were not available for this study. Using an updated binned model, however, would not affect

the primary conclusions of this study. As additional bins are added, the characteristic area model will approach the correlated length model.

Acknowledgments

This work was partially supported by National Science Foundation (NSF) Grant Numbers OCE1130013, OCE1147975, and OCE1355878. We thank Allan Lindh, Associate Editor Delphine Fitzenz, and an anonymous reviewer for detailed questions and comments that led to a clearer, more concise article. Paul Somerville, Chris Goldfinger, and Lingling Ye kindly provided tabulated data that facilitated this analysis.

References

Aki, K. (1965). Maximum likelihood estimate of b in the formula $\log N = a - bM$ and its confidence limits, *Bull. Earthq. Res. Inst.* **43,** 237–239.

Atwater, B. F., and G. B. Griggs (2012). Deep-sea turbidites as guides to Holocene earthquake history at the Cascadia subduction zone—Alternative views for a seismic hazard workshop, *U.S. Geol. Surv. Open-File Rept. 2012-1043*, 58 pp.

Boyarko, D. C., M. R. Brudzinski, R. W. Porritt, R. M. Allen, and A. M. Tréhu (2015). Automated detection and location of tectonic tremor along the entire Cascadia margin from 2005 to 2011, *Earth Planet. Sci. Lett.* **430,** 160–170.

Burgette, R. J., R. J. Weldon II, and D. A. Schmidt (2009). Interseismic uplift rates for western Oregon and along-strike variation in locking on the Cascadia subduction zone, *J. Geophys. Res.* **114,** no. B01408, doi: 10.1029/2008JB005679.

Chapman, J., and T. Melbourne (2009). Future Cascadia megathrust rupture delineated by episodic tremor and slip, *Geophys. Res. Lett.* **36,** L22301, doi: 10.1029/2009GL040465.

Comte, D., and M. Pardo (1991). Reappraisal of great historical earthquakes in the northern Chile and southern Peru seismic gaps, *Nat. Hazards* **4,** 23–44.

Goldfinger, C., C. H. Nelson, A. Morey, J. E. Johnson, J. Gutierrez-Pastor, A. T. Eriksson, E. Karabanov, J. Patton, E. Gracia, G. Dunhill, *et al.* (2012). Turbidite event history: Methods and implications for Holocene paleoseismicity of the Cascadia subduction zone, *U.S. Geol. Surv. Profess. Pap. 1661-F*, U.S. Geological Survey, Reston, Virginia, 332 pp.

Hyndman, R. D. (2013). Downdip landward limit of Cascadia great earthquake rupture, *J. Geophys. Res.* **118,** 5530–5549, doi: 10.1002/jgrb.50390.

Hyndman, R. D., and K. Wang (1993). Thermal constraints on the zone of major thrust earthquake failure—The Cascadia subduction zone, *J. Geophys. Res.* **98,** 2039–2060.

Kanamori, H., and D. L. Anderson (1975). Theoretical basis of some empirical relations in seismology, *Bull. Seismol. Soc. Am.* **65,** 1073–1095.

Kulkarni, R., I. Wong, J. Zachariasen, C. Goldfinger, and M. Lawrence (2013). Statistical analyses of great earthquake recurrence along the Cascadia subduction zone, *Seismol. Soc. Am. Bull.* **103,** 3205–3221.

Leonard, L. J, C. A. Currie, S. Mazzotti, and R. D. Hyndman (2010). Rupture area and displacement of past Cascadia great earthquakes from coastal coseismic subsidence, *Geol. Soc. Am. Bull.* **122,** nos. 11/12, 2079–2096, doi: 10.1130/B30108.1.

McCaffrey, R., A. I. Qamar, R. W. King, R. Wells, G. Khazaradze, C. A. Williams, C. W. Stevens, J. J. Vollick, and P. C. Zwick (2007). Fault locking, block rotation and crustal deformation in the Pacific Northwest, *Geophys. J. Int.* **169,** 1315–1340.

Naylor, M., K. Orfanogiannaki, and D. Harte (2010). Exploratory data analysis: Magnitude, space, and time, *Community Online Resource for Statistical Seismicity Analysis*, doi: 10.5078/corssa-92330203, http://www.corssa.org (last accessed November 2015).

Nishikawa, T., and S. Ide (2014). Earthquake size distribution in subduction zones linked to slab buoyancy, *Nat. Geosci.* **7,** 904–908, doi: 10.1038/NGEO2279.

Petersen, M. D., M. P. Moschetti, P. M. Powers, C. S. Mueller, K. M. Haller, A. D. Frankel, Y. Zeng, S. Rezaeian, S. C. Harmsen, O. S. Boyd, *et al.* (2014). Documentation for the 2014 update of the United States national seismic hazard maps, *U.S. Geol. Surv. Open-File Rept. 2014-1091*, 243 pp., doi: 10.3133/ofr20141091.

Rong, Y., D. D. Jackson, H. Magistrale, and C. Goldfinger (2014). Magnitude limits of subduction zone earthquakes, *Bull. Seismol. Soc. Am.* **104,** no. 5, 2359, doi: 10.1785/0120130287.

Satake, K., K. Wang, and B. F. Atwater (2003). Fault slip and seismic moment of the 1700 Cascadia earthquake inferred from Japanese tsunami descriptions, *J. Geophys. Res.* **108,** 2325, doi: 10.1029/2003JB002521.

Scholz, C. H. (1994). A reappraisal of large earthquake scaling, *Bull. Seismol. Soc. Am.* **84,** 215–218.

Scholz, C. H. (2002). *The Mechanics of Earthquakes and Faulting*, Second Ed., Cambridge University Press, Cambridge, United Kingdom, 471 pp.

Scholz, C. H. (2014). Holocene earthquake history of Cascadia: A quantitative test, *Bull. Seismol. Soc. Am.* **104,** no. 4, 2120, doi: 10.1785/0120140002.

Scholz, C. H., and J. Campos (2012). The seismic coupling of subduction zones revisited, *J. Geophys. Res.* **117,** no. B05310, doi: 10.1029/2011JB009003.

Schmalzle, G. M., R. McCaffrey, and K. C. Creager (2014). Central Cascadia subduction zone creep, *Geochem. Geophys. Geosys.* **15,** no. 4, 1515–1532, doi: 10.1002/2013GC005172.

Skarlatoudis, A. A., P. G. Somerville, H. K. Thio, and J. R. Bayless (2015). Broadband strong ground motion simulations of large subduction earthquakes, *Bull. Seismol. Soc. Am.* **105,** no. 6, doi: 10.1785/0120140322.

Somerville, P., A. Skarlatoudis, and H. K. Thio (2015). Source scaling relations of subduction earthquakes for strong ground motion and tsunami prediction, *Final Rept., U.S. Geol. Surv. Award G13AP00028*, 25 pp.

Wang, K., and A. M. Tréhu (2016). Invited review paper: Some outstanding issues in the study of great megathrust earthquake—The Cascadia example, *J. Geodyn.* **97,** doi: 10.1016/j.jog.2016.03.010.

Wang, P.-L., S. E. Engelhart, K. Wang, A. D. Hawkes, B. P. Horton, A. R. Nelson, and R. C. Witter (2013). Heterogeneous rupture in the great Cascadia earthquake of 1700 inferred from coastal subsidence estimate, *J. Geophys. Res.* **118,** no. 5, 2460–2473, doi: 10.1002/jgrb.50101.

Ye, L., T. Lay, H. Kanamori, and L. Rivera (2016). Rupture characteristics of major and great ($M_w \geq 7.0$) megathrust earthquakes from 1990 to 2015: 1. Source parameter scaling relationships, *J. Geophys. Res.* **121,** no. 2, 826–844, doi: 10.1002/2015JB012426.

College of Earth Ocean and Atmospheric Science
Oregon State University
104 CEOAS Admin. Bld.
101 SW 26th Street
Corvallis, Oregon 97331-5503
trehu@coas.oregonstate.edu

Manuscript received 31 March 2016;
Published Online 24 May 2016